Processing and Application of Ceramics 16 [3] (2022) 259–266
https://doi.org/10.2298/PAC2203259M

Study of milling time impact on hydrogen desorption from $LiAlH_4$-Fe_2O_3 composites

Igor Milanović[1], Sanja Milošević Govedarović[1], Miodrag Lukić[2,3], Zoran Jovanović[1], Jelena Rmuš[1], Anđela Mitrović Rajić[1], Jasmina Grbović Novaković[1], Sandra Kurko[1,*]

[1]*Centre of Excellence for Renewable and Hydrogen Energy, "Vinča" Institute of Nuclear Sciences, National Institute of Republic of Serbia, University of Belgrade, Mike Petrovića Alasa 12-14, POB 522, 11001 Belgrade, Serbia*
[2]*Institute of Inorganic Chemistry, Leibniz University Hannover, 30167 Hannover, Germany*
[3]*Centre for Fine Particles Processing and Nanotechnologies, Institute of Technical Sciences of the Serbian Academy of Sciences and Arts, Knez Mihailova 35/IV, Belgrade 11000, Serbia*

Received 24 November 2021; Received in revised form 16 May 2022; Accepted 18 August 2022

Abstract

$LiAlH_4$ was modified by mechanical milling and with the addition of 5 wt.% Fe_2O_3 in order to improve its hydrogen desorption properties. The composite was milled for 1, 3, 5, 7 or 15 min, and depending on the milling time, various phenomena took place. Up to a milling time of 5 min, the particle size of the composite decreases. Further milling leads to the particles agglomeration reaching the size of the starting material after 15 min. Moreover, the mechanical milling process leads to the transformation of AlH_4^- to AlH_6^{3-} structure as a result of partial hydrogen desorption. Hydrogen desorption during the milling is the most pronounced in the sample milled for 15 min, so this sample has only one hydrogen desorption peak in the temperature-programmed desorption measurements. Mechanical milling with the addition of Fe_2O_3 for up to 15 min improves $LiAlH_4$ hydrogen desorption properties as hydrogen desorption temperature and apparent activation energies decrease.

Keywords: *hydrides, composites, mechanochemical synthesis, hydrogen storage, kinetics*

I. Introduction

Metal and complex light hydrides are the best-fitted materials for hydrogen storage within the concept of hydrogen-based economy [1,2]. These materials meet the basic application requirements: low-cost, safe usage (stable compounds and composites based on them), and they are environmentally friendly (reversible materials with a few thousands of sorption cycles lifespan). However, as relatively stable compounds they exhibit some undesirable properties such as sluggish dehydrogenation kinetics and high hydrogen desorption temperature. Among various hydrides, $LiAlH_4$ (space group $P2_1/c$) emerged as an attractive candidate for solid-state hydrogen storage at moderate pressures and temperatures [3]. This compound decomposes in three steps, according to the following reactions [3,4]:

$$3\,LiAlH_4 \longrightarrow Li_3AlH_6 + 2\,Al + 3\,H_2 \qquad (R1)$$

$$Li_3AlH_6 \longrightarrow 3\,LiH + Al + \frac{3}{2}\,H_2 \qquad (R2)$$

$$3\,LiH + 3\,Al \longrightarrow 3\,LiAl + \frac{3}{2}\,H_2 \qquad (R3)$$

The first reaction occurs in the temperature range of 150–175 °C, the second between 180–220 °C and the third one between 400–420 °C. The first two reactions are significant from the hydrogen storage point of view: i) both take place at a reasonably low temperature (R2 ends at 220 °C) and ii) the overall sum of their gravimetric hydrogen capacity is 7.9 wt.%. Thus, the reactions R1 and R2 are accessible for practical hydrogen storage. However, slow hydrogen desorption kinetics of the pure hydride and irreversibility of cycling are still bottlenecks for the on-board application of lithium-alanate.

*Corresponding author: tel: +381 64 1745 363
e-mail: *skumric@vin.bg.ac.rs*

Nevertheless, $LiAlH_4$ is suitable for synthesizing the composites with 5 or 10 wt.% of additive. The additive should improve the dehydrogenation process of hydride without a significant decrease in storage capacity, so these composites could still meet the US DoE's target of 5.5 wt.% H_2 storage capacity for practical application [5].

Various additives like pure metals [6–8], carbides [9,10], halides [11–15], carbon based materials [16], metallic oxides and oxide ceramics [17–24] and hydrides [12,25] were used in order to improve the hydrogen sorption properties of $LiAlH_4$. These improvements are achieved due to the reduction of the particle size of hydrides to the nanoscale, an increase in reactive particle surface area, destabilization of the hydride crystal structure and catalytic performance of additives. Li *et al.* [17] showed that the onset dehydrogenation temperature is about 80 °C lower for the reaction R1 and 45–60 °C lower for the second stage (R2) when 5 mol% of Fe_2O_3 and Co_2O_3 are added to $LiAlH_4$. The addition of these oxides also improves the reaction kinetics. The composites release 7.1 wt.% of hydrogen in 70 min (at 120 °C), compared to the as-received $LiAlH_4$ that desorbs 0.3 wt.% of H_2 under the same conditions. So, the apparent activation energies (E_{aap}) for both desorption steps are considerably lower than in the pure $LiAlH_4$. Doping with Fe-Fe_2O_3 promotes formation of Fe-Al and Fe-Al_2O_3 intermetallics during dehydrogenation of $LiAlH_4$. These phases have beneficial impact on the hydrogen desorption kinetics by promoting diffusion of hydrogen ions [22]. Ismail *et al.* [21] have demonstrated that adding a small amount of TiO_2 to $LiAlH_4$ results in a significant 90 °C reduction in the decomposition temperature compared to the as-received $LiAlH_4$. The composite material starts releasing hydrogen at 60 °C, so dehydrogenation is completed below 200 °C, with approximately 7.5 wt.% of H_2 desorbed. Changing TiO_2 to Sr-titanate also decreases both the hydrogen release temperature and activation energies [23]. When added 7 wt.% of $NiTiO_3$@h-BN to $LiAlH_4$ the R1 starts at 68 °C, and activation energies for both R1 and R2 are significantly reduced. The absorption of hydrogen at 30 bar and 300 °C achieved approximately 1 wt.% [24]. In $LiAlH_4$ composite with 10 wt.% of K_2NbF_7 activation energies decreased for 24 (R1) and 26 kJ/mol (R2) compared to the as-milled $LiAlH_4$. Improvement in the desorption kinetics performance was attributed to the *in situ* formation of NbF_4, LiF and K or K-containing phases that appeared during the heating process [11]. On the other hand in $LiAlH_4$ doped with K_2NiFe_6, AlNi and LiF phases formed during dehydrogenation and improved its kinetics [15]. Similarly, by milling $LiAlH_4$ with 7 wt.% of $NiFe_2O_4$ [18], hydrogen desorption energies were reduced by approximately 60%. Desorption energy barrier decreased because *in situ* formed Al_4Ni_3 accelerates the breakdown of Al-H bonding through the interfacial charge transfer and the dehybridization of Al-H cluster. It supports our previous findings that the charge transfer from $LiAlH_4$ and Li_3AlH_6 to Fe_2O_3 leads to weaker bonding of hydrogen atoms and improved hydrogen desorption performance of $LiAlH_4$ [26].

High-energy ball milling proved to be the best method for the composite synthesis and additives and defects introduction in the $LiAlH_4$ structure. However, composites often desorb less hydrogen than expected, especially under prolonged milling conditions [27]. During the milling process, the temperature in the milling chamber can significantly increase, reaching the temperature of R1 or even R2 leading to the degradation of hydride and the decrease in the hydrogen storage capacity of the material. Prevention of the hydride decomposition during the preparation was done in cryogenic ball-milling [12,13]. But this process requires the liquid nitrogen temperature. So, in this work, we studied the impact of the milling time on the hydride structure, possible degradation, and desorption properties in lithium alanate/iron(III)-oxide composites (5 wt.%).

II. Experimental

The $LiAlH_4$ + 5 wt.% Fe_2O_3 (labelled as LiFe) composites were synthesized by mechanochemical milling in high-energy ball mill SPEX 5100 using hardened steel ball and the ball to powder ratio (BPR) 10:1. The mass of the ball was 1 g, so 100 mg of composite was synthesized after one process. Used chemicals are Alfa Aesar $LiAlH_4$ (purity 97%) and catalyst grade Sigma Aldrich Fe_2O_3. The samples were milled for 1, 3, 5, 7 and 15 min. The sample labels are given in the Table 1. Handling of the samples and milling processes were done in the argon atmosphere.

Structural and phase characterization were done using Ultima IV Rigaku X-ray diffractometer. The diffractometer was equipped with Cu $K_{\alpha 1,2}$ radiation source, with voltage of 40.0 kV and a current of 40.0 mA. Diffractograms were recorded in 2θ range from 10 to 80°, with recording step of 0.02° and scanning rate of

Table 1. The sample labels

Sample mark	$LiAlH_4$ [wt.%]	Fe_2O_3 [wt.%]	Milling time [min]
$LiAlH_4$ as-received	100	0	0
LiFe1	95	5	1
LiFe3	95	5	3
LiFe5	95	5	5
LiFe7	95	5	7
LiFe15	95	5	15

2°/min. The morphology of materials surface and their microstructure were characterized by scanning electron microscope SEM, JEOL JSM 6460LV equipped with EDS INCA microanalysis. A quantitative particle size distribution was obtained by Malvern 2000 SM Mastersizer laser scattering particle size analysis system. The specified resolution range of the system was sub-μm to 2 mm. 2-propanol was used as a suspension media. To enhance the dispersion, all samples were ultrasonicated for 5 min prior to measurements. The same stirring speed and obscuration level were used for all samples. Fourier transform infrared spectroscopy (FTIR) was used for analysis of the pure and doped $LiAlH_4$ samples using a Perkin Elmer Spectrum Two FT-IR spectrometer using the pressed KBr pellets technique (mass ration 1:100). Range of the recording was from 800 to 2000 cm^{-1} with a spectral resolution of 2 cm^{-1}. Thermal behaviour of the samples was investigated by temperature programmed desorption (TPD). A custom-built set-up for TPD was used. The composites of lithium alanates doped with iron(III)-oxide in the form of powders were put in the sample holder made of quartz. Quartz tube was placed inside an electrical furnace and coupled with an Extorr 3000 quadrupole mass spectrometer (Extorr Inc.). The signals, as partial pressures (torr) at 7 different m/z ratios were followed and simultaneously recorded as a function of time (s): 1 (H), 2 (H_2), 17 (NH_3 or OH), 18 (H_2O), 28 (CO), 32 (O_2), 44 (CO_2). Up to 5 mg of the samples were placed in the quartz tube, outgassed to 10^{-7} torr and then subjected to TPD at a linear heating rate of 10 °C/min, from room temperature to 350 °C.

III. Results and discussion

3.1. Microstructural characterization

X-ray diffraction patterns of the as-received (unmilled) $LiAlH_4$, Fe_2O_3 and their composites $LiAlH_4$-5 wt.% Fe_2O_3 milled for 1, 3, 5, 7 and 15 min are shown in Fig. 1. All characteristic $LiAH_4$ peaks are observed in the 2θ range from 20 to 50° and correspond to monoclinic unit cell ($P2_1/c$) [28]. The as-received hydride has also small amount of Al phase impurity, whose characteristic maxima are at 38.5 and 44.5° [27]. There are no visible peaks from oxide or hydroxide impurities [29,30]. The composite samples show diffraction maxima originating from $LiAlH_4$ and Fe_2O_3 phase. As milling time increases the intensity of characteristic lithium-alanate phase maxima decreases and becomes broader. After 15 min of high energy milling, there are no visible $LiAlH_4$ phase peaks. On the other hand, intensity of aluminium peaks increases, indicating the hydride decomposition. There is also broad peak in the sample milled for 15 min at approximately 22° that could correspond to Li_3AlH_6 phase maxima at 21.95° and 22.55° [27]. The structure of $LiAlH_4$ is prone to destabilization by mechanochemical treatment, so this phase transformation happens if desorption of H_2 (reaction R1) takes place during milling [27,28]. During this transformation lithium hexahydridoaluminate (Li_3AlH_6) and Al phases are gradually generated. The characteristic Fe_2O_3 peaks also become more pronounced with the milling time increase [17].

The reduction in hydride crystallite size in the composite upon milling for various times is calculated by Debye-Scherrer equation from the broadening of 101 peak and the results are presented in Table 2 [31]. It can be seen that 3 min of milling leads to the decrease in crystallite size for 32%, while further milling does not have any effect. The shape of the unmilled $LiAlH_4$ particles is relatively regular with sharp edges that resemble the monoclinic crystal lattice of hydride (Fig. 2a). The particle size distribution is uniform. The ball milling impact on the hydride particle morphology is visible in Figs. 2c,d for the composite milled for 5 min. Milling

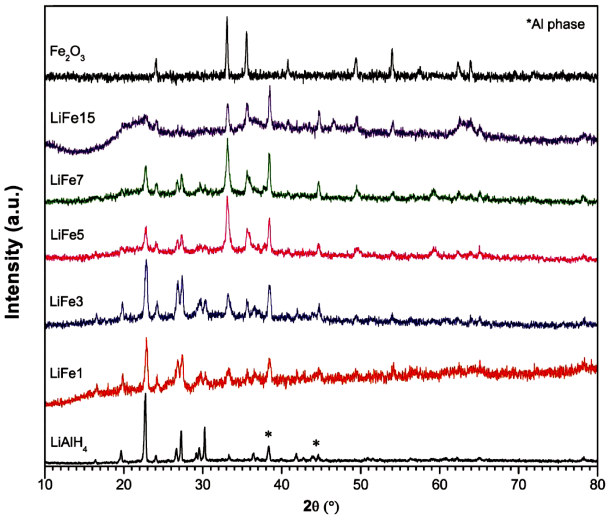

Figure 1. XRD patterns of unmilled $LiAlH_4$ and Fe_2O_3 phases and $LiAlH_4$-Fe_2O_3 composites milled for 1 (LiFe1), 3 (LiFe3), 5 (LiFe5), 7 (LiFe7) and 15 min (LiFe15)

Table 2. Interplanar distance (d), crystallite size (D) and mean particle size of as-received $LiAlH_4$ and composite samples

Sample	2θ [°]	d [Å]	D [nm]	Mean particle size [μm] (left/right peak)
$LiAlH_4$	22.68	3.917	33	22
LiFe1	22.74	3.907	25	12/130
LiFe3	22.79	3.899	22	6/145
LiFe5	22.77	3.902	24	5/20
LiFe7	22.79	3.899	24	12
LiFe15	22.79	3.899	7	23

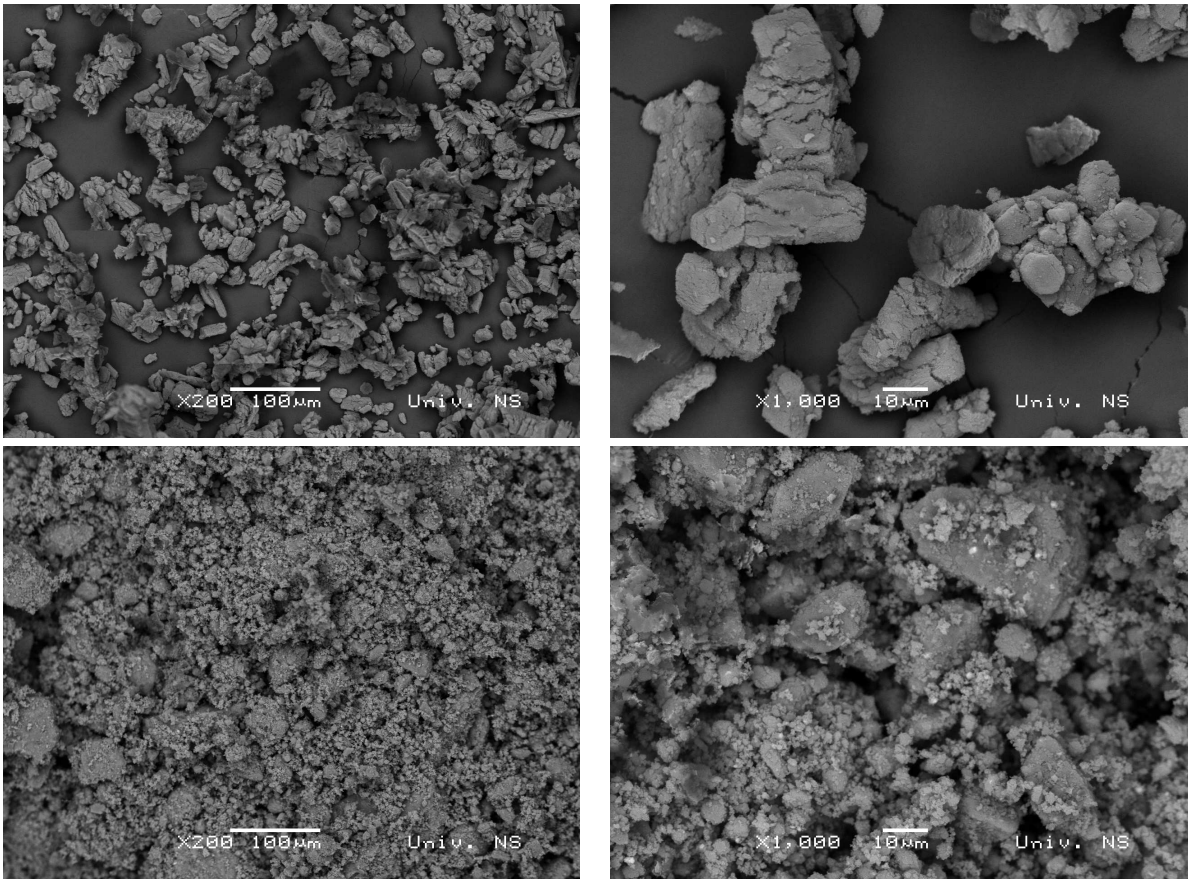

Figure 2. SEM micrographs of unmilled $LiAlH_4$ (a and b) and $LiAlH_4$-Fe_2O_3 composite milled for 5 min - LiFe5 (c and d)

led to the significant refinement of particles. Milled particles have irregular shape with sponge-like structure and broad particle size distribution. There is also visible agglomeration of particles in the milled sample.

The results of the particle size distribution obtained by laser scattering (LS) measurements are presented in Fig. 3. In the unmilled $LiAlH_4$ the 99% of sample volume consists of particles in the range between 1 and 100 μm with the mean particle size of 22 μm. Distribution of particles is not fully monomodal, but there is a shoulder in the range between 1 and 10 μm with the maximum at 3 μm. The sample LiFe1 shows bimodal distribution of particles in the range from 300 nm to 300 μm, where 73% of the volume consists of smaller particles with the mean size of 12 μm while 27% of particles are between 100 and 300 μm, with the mean particle size of 130 μm. In comparison to the unmilled $LiAlH_4$, main peak is shifted to smaller particles in the range from 22 to 12 μm. The composite milled for 3 min, LiFe3, shows also bimodal distribution: 86% of particle volume is in the range from 1 to 100 μm with the mean particle size of 6 μm, while 14% of volume is between 100 and 200 μm (mean particle size 145 μm). In the LiFe5 sample 0.2% of particles volume is in the range from 250 nm to 1 μm, 78% in the range from 1 to 100 μm and 21.8% between 100 μm to 300 μm. Distribution is bimodal with the two peaks maxima at 5 and 20 μm. PSD analysis of the LiFe7 shows only one peak which characterizes very high symmetry (bell-like shape). Almost all the particles are distributed in the range from 1 to 100 μm (97.2% of particles) and rest of particles are distributed in range from 100 to 160 μm (2.8% of particles). Mean particle size is 12.5 μm. The LiFe15 composite has also monomodal distribution, but the mean particle size is 23 μm. All particles are distributed in the range from 0.5 to 100 μm. The milling process leads to the decrease of particle size up to 5 min

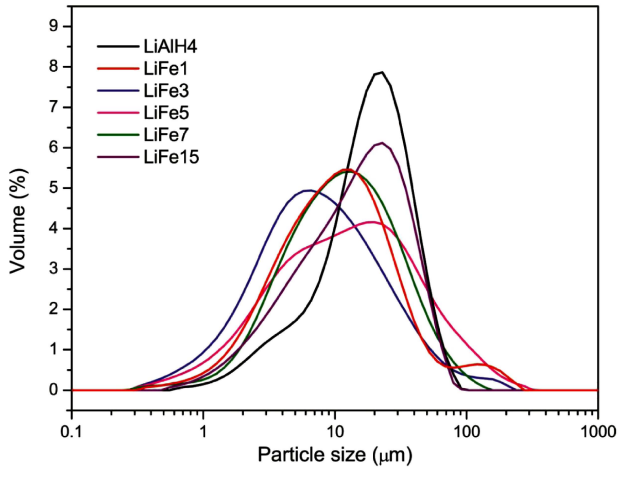

Figure 3. Particle size distribution (PSD) of unmilled $LiAlH_4$ and $LiAlH_4$-Fe_2O_3 composites milled for 1 (LiFe1), 3 (LiFe3), 5 (LiFe5), 7 (LiFe7), and 15 min (LiFe15)

milling, afterwards particles start to agglomerate. Up to 7 min milling there are two types of particles: bigger and smaller than 100 μm. It is interesting that after 7 min of milling, distribution is monomodal and almost without particles bigger than 100 μm, which is similar in the sample milled for 15 min. The mean particle size in the composite milled for 15 min is similar to the mean particle size of the starting hydride.

Fourier transform infrared (FTIR) spectra of the as-received $LiAlH_4$ and milled $LiAlH_4$-5 wt.% Fe_2O_3 composites are shown in Fig. 4. Whole spectrum is in the 800–2000 cm^{-1} wavenumber range. $LiAlH_4$ has two active infrared vibrations: Al–H stretching mode at 1641 cm^{-1} and Li–Al–H bending mode at 885 cm^{-1} [17]. As milling starts, the stretching mode becomes less pronounced with the appearance of Al–H stretching mode from hexahydridoaluminate ions (AlH_6^{3-}) in Li_3AlH_6 at 1385 and 1500 cm^{-1} [14,17]. This peak increases with the milling time indicating decomposition of $LiAlH_4$ via reaction R1 which is in accordance with XRD findings. So, the addition of Fe_2O_3 facilitates the H_2 release from $LiAlH_4$ and the dehydrogenation process begins very fast when milling in high energy mill starts.

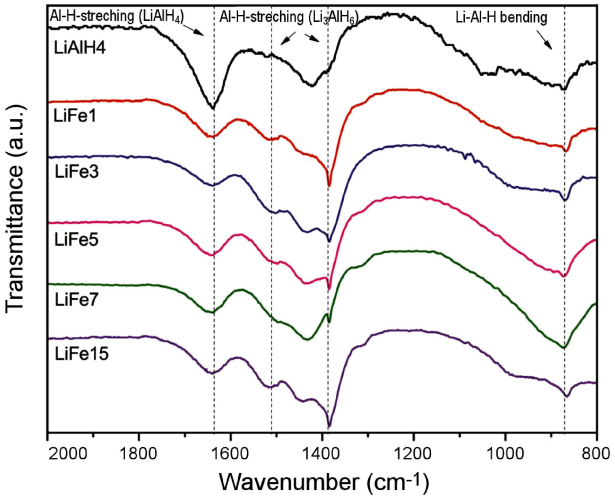

Figure 4. FTIR of the unmilled $LiAlH_4$ and $LiAlH_4$-5 wt.% Fe_2O_3 composites milled for 1 (LiFe1), 3 (LiFe3), 5 (LiFe5), 7 (LiFe7) and 15 min (LiFe15)

3.2. Analysis of dehydrogenation properties

To study the dehydrogenation properties of the pure $LiAlH_4$ and composite materials milled for different times, TPD-MS was done. Desorption of hydrogen obtained from TPD measurements is presented in Fig. 5. As shown in Fig. 5, there are two distinguished H_2 desorption maxima for the unmilled $LiAlH_4$ at 137 (LT) and 143 °C (HT) corresponding to the reactions R1 and R2, respectively. There is also very small peak at 132.5 °C which could originate from the smaller particles (1–10 μm) that form shoulder in particle size distribution (Fig. 2) in this sample. The addition of 5 wt.% Fe_2O_3 by mechanical milling leads to the decrease in hydrogen desorption temperature and the dependence of hydrogen desorption temperature on time can be noticed. The one minute milled $LiAlH_4$-5 wt.% Fe_2O_3 composite, LiFe1, releases hydrogen at 124 and 133 °C, but the first peak at lower temperature (LT) is smaller than the second one.

After 3 min of milling, the composite releases hydrogen at 126 and 137 °C with the higher amount of hydrogen desorbed by reaction R1. The further milling time increase, up to 15 min, does not influence the desorption temperature to a large extent, but it changes the portions of hydrogen released by reactions R1 and R2. Finally, 15 min of milling leads to the one step hydrogen desorption. As XRD and FTIR analyses showed, there is certain H_2 release during the milling process by reaction R1, where the destabilized structure of $LiAlH_4$ phase decomposes to lithium hexahydridoaluminate phase [27]. This is the most pronounced in the composite milled for 15 min, so the TPD single peak can be attributed to the hydrogen release completely by only reaction R2.

Kinetics and mechanism of the solid-state reactions can be modelled with a few models depending on the sorption reaction limiting step [32]. Šestak and Berggren [33] explored the possibility to obtain the

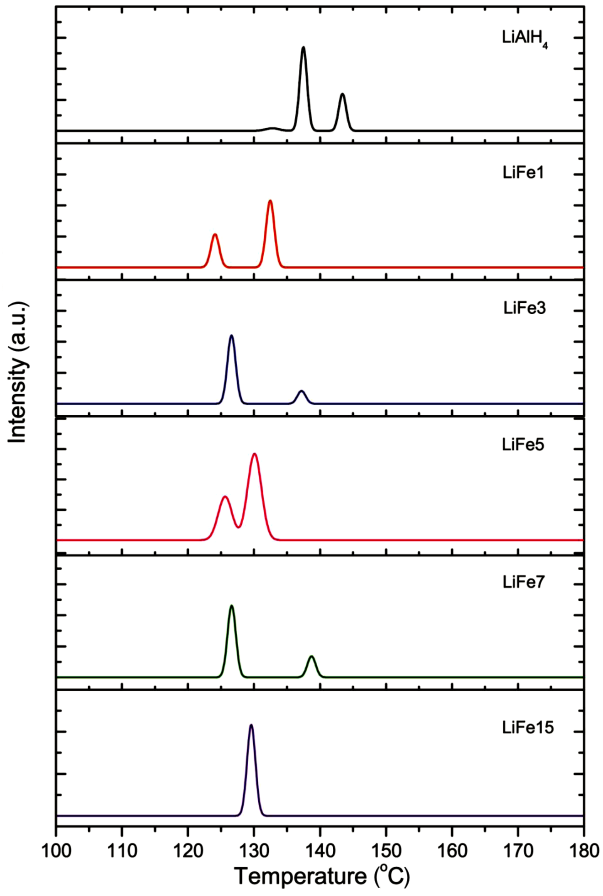

Figure 5. Temperature programmed desorption (TPD) spectra of the unmilled $LiAlH_4$ and $LiAlH_4$-5 wt.% Fe_2O_3 composites milled for 1 (LiFe1), 3 (LiFe3), 5 (LiFe5), 7 (LiFe7), and 15 min (LiFe15)

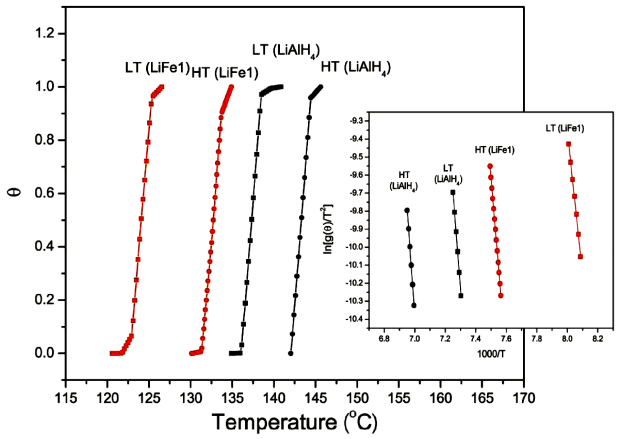

Figure 6. Temperature evolution of the reacted fraction (θ) corresponding to $LiAlH_4$ hydrogen desorption, obtained by integration of TPD peaks for unmilled hydride ($LiAlH_4$) and composite LiFe1 milled for 1 min (insert: experimental data and the best fit obtained for nucleation and growth model $g(\theta) = [-\ln(1-\theta)]^{1/2}$)

mechanism of thermal decomposition process from the non-isothermal curves. Detailed application of this method on the reaction of hydrogen desorption from hydrides is given in our previous work [32]. Desorption curves of the $LiAlH_4$ and its composites with Fe_2O_3, have been analysed using different kinetic models. The analysis of TPD curves indicates that the H_2 desorption from the $LiAlH_4$ and its composites with Fe_2O_3 are controlled by nucleation and growth mechanisms with the Avrami parameter $n = 2$ over a coverage θ range from 0.3 to 0.8 (Fig. 6).

Parameter $n = 2$ corresponds to two-dimensional (2D) nuclei growth. In this model, the reacted fraction θ can be related to temperature (T) by:

$$\ln\left[\frac{[-\ln(1-\theta)]^{1/n}}{T^2}\right] = f\left(\frac{1000}{T}\right) \quad (1)$$

Calculated apparent activation energies E_{aap} (kJ/mol) for all samples and both hydrogen desorption steps (reactions R1 and R2) are given in Table 3.

It can be seen that mechanical milling of the composite with Fe_2O_3 even as short as one minute significantly improves the kinetics of reactions R1 and R2. The lowest desorption temperatures and apparent activation energies E_{app} are in the composite sample milled for five minutes. The values of apparent activation energies are comparable to the ones found in the literature obtained by the Kissinger method (Table 4). In our previous work, we have discussed the role of Fe_2O_3 on hydrogen desorption from $LiAlH_4$ [26]. We showed that a significant portion of the iron ions has changed their valence state from Fe^{3+} to the Fe^0 and Fe^{2+} after hydride decomposition, so there is a transfer of an electron to Fe_2O_3 during hydrogen desorption. The effect of charge transfer from $LiAlH_4$ and Li_3AlH_6 to Fe_2O_3 leads to weaker bonding of hydrogen atoms and easier hydrogen desorption.

IV. Conclusions

The presented results lead to conclusion that the composite of $LiAlH_4$ with Fe_2O_3 milled for as short as 1 min in a high energy mill shows significantly better desorption properties than the unmilled $LiAlH_4$, i.e. i) temperature peaks of hydrogen desorption are shifted to lower positions for all composites; ii) increase of milling time

Table 3. H_2 desorption temperature and apparent activation energy obtained from TPD measurements (LT - lower temperature peak, HT - higher temperature peak)

Sample	Temperature (LT) [°C]	$E_{aap,LT}$ [kJ/mol]	Temperature (HT) [°C]	$E_{aap,HT}$ [kJ/mol]
$LiAlH_4$	137	91 ± 1	143	98 ± 1
LiFe1	124	66 ± 2	133	83.2 ± 0.3
LiFe3	126	77 ± 1	137	88 ± 0.5
LiFe5	125	55 ± 2	130	69 ± 3
LiFe7	127	72 ± 1	139	89 ± 1
LiFe15	129	70 ± 3	-	-

Table 4. Apparent activation energy (E_{aap}) of as-received $LiAlH_4$ and $LiAlH_4$ doped with various catalysts, calculated by the Kissinger method

E_{aap} [kJ/mol] (LT/HT)	Compound	Experimental conditions	Reference
81/108	$LiAlH_4$	As received	[8]
89/103	$LiAlH_4$ - 2 mol% $TiCl_3$*1/3$AlCl_3$	Milled for 1 min	
100/130	$LiAlH_4$	Milled for 90 min	[27]
80/100	$LiAlH_4$ - 5 wt.% 2 DTi_2C_3	Milled for 10 h	[10]
111/100	$LiAlH_4$	As received	[34]
92.5/92	$LiAlH_4$	Milled for 15 min	
102/110	$LiAlH_4$	As received	[20]
84/96	$LiAlH_4$ - 5 wt.% Fe_2O_3	Milled for 60 min	
95/172	$LiAlH_4$	As received	
54/86	$LiAlH_4$ - 5 mol% Fe_2O_3	Milled for 30 min	[17]
56/93	$LiAlH_4$ - 5 mol% Cr_2O_3	Milled for 30 min	

causes the change in the intensity of two characteristic hydrogen desorption peaks; iii) the activation energy for all milled composites is lower in comparison to the unmilled $LiAlH_4$. During the process of high energy mechanical milling, hydrogen desorption by R1 reaction starts, so the composites milled for 15 min have only one desorption maxima corresponding to R2 reaction. Using the ball milling approach to synthesize the nanostructured hydrides can significantly enhance the thermodynamics and kinetics of dehydrogenation. However, there is necessary to apply the minimal milling time. This minimal milling time should be long enough to assure the best composite properties, but not to start the hydrogen desorption. For explored milling conditions (experimental part) optimal results are obtained in the sample milled for 5 min. It is assumed that this milling time is long enough to disperse the catalyst homogeneously around $LiAlH_4$ particles and also cause the maximal reduction in the particle size. Further milling leads to the particle agglomeration, but more importantly to the significant hydrogen release during milling.

Acknowledgement: This research was financially supported by The Ministry of Education, Science and Technology of the Republic of Serbia through the Program of institutional financing

References

1. A. Züttel, A. Remhof, A. Borgschulte, O. Friedrichs, "Hydrogen: the future energy carrier", *Philos. T. R. Soc. A*, **368** [1923] (2010) 3329–3342.
2. E. Boateng, A. Chen, "Recent advances in nanomaterial-based solid-state hydrogen storage", *Mater. Today Adv.*, **6** (2020) 100022.
3. N.A. Sazelee, M. Ismail, "Recent advances in catalyst-enhanced $LiAlH_4$ for solid-state hydrogen storage: A review", *Int. J. Hydrogen Energy*, **46** (2021) 9123–9141.
4. J.A. Dilts, E.C. Ashby, "Thermal decomposition of complex metal hydrides", *Inorg. Chem.*, **11** [6] (1972) 1230–1236.
5. U.S. Department of Energy, *Fuel Cell Technologies Office Multi-Year Research, Development, and Demonstration Plan*, 2014. Available online: `DoE link`.
6. P.B. Amama, J.T. Grant, P.J. Shamberger, A.A. Voevodin, T.S. Fishe, "Improved dehydrogenation properties of Ti doped $LiAlH_4$: Role of Ti precursors", *J. Phys. Chem. C*, **116** (2012) 21886–21894.
7. R.A. Varin, R. Parviz, "The effects of the micrometric and nanometric iron (Fe) additives on the mechanical and thermal dehydrogenation of lithium alanate ($LiAlH_4$), its self-discharge at low temperatures and rehydrogenation", *Int. J. Hydrogen Energy*, **37** (2012) 9088–9102.
8. A. Andreasen, "Effect of Ti-doping on the dehydrogenation kinetic parameters of lithium aluminum hydride", *J. Alloys Compd.*, **419** [1] (2006) 40–44.
9. Z.L. Li, F.Q. Zhai, H.C. Qiu, Q. Wan, P. Li, X.H. Qu, "Dehydrogenation characteristics of ZrC-doped $LiAlH_4$ with different mixing conditions", *Rare Met.*, **39** (2020) 383–391.
10. Y. Xia, H. Zhang, Y. Sun, L. Sun, F. Xu, S. Sun, G. Zhang, P. Huang, Y. Du, J. Wang, S.P. Verevkin, A.A. Pimerzin, "Dehybridization effect in improved dehydrogenation of $LiAlH_4$ by doping with two-dimensional Ti_3C_2", *Mater. Today Nano*, **8** (2019) 100054.
11. N.A. Ali, N. Sazelee, M.S. Yahya, M. Ismail, "Influence of K_2NbF_7 catalyst on the desorption behavior of $LiAlH_4$", *Front. Chem.*, **8** (2020) 457.
12. J.R. Tena-García, R.D. Poiré de la Cruz, K. Suárez-Alcántara, "On the dehydrogenation of $LiAlH_4$ enhanced by Ti salts and cryogenic ball-milling", *Int. J. Hydrogen Energy*, **45** (2020) 19431–19439.
13. J.R. Tena-García, A. Casillas-Ramírez, R. Guerrero-Ortiz, D.R. Poiré de la Cruz, K. Suarez-Alcantara, "$LiAlH_4$–$ZrCl_4$ mixtures for hydrogen release at near room temperature", *Int. J. Hydrogen Energy*, **47** (2022) 30234–30247.
14. J. Ares Fernandez, F. Aguey-Zinsou, M. Elsaesser, X.Z. Ma, M. Dornheim, T. Klassen, R. Bormann, "Mechanical and thermal decomposition of $LiAlH_4$ with metal halides", *Int. J. Hydrogen Energy*, **32** [8] (2007) 1033–1040.
15. M.A.N. Ahmad, N.A. Sazelee, N.A. Ali, M. Ismail, "Enhancing the dehydrogenation properties of $LiAlH_4$ using K_2NiF_6 as additive", *Int. J. Hydrogen Energ.*, **47** [59] (2022) 24843–24851.
16. J. Ye, G. Xia, X. Yu, "In-situ constructed destabilization reaction of $LiBH_4$ wrapped with graphene toward stable hydrogen storage reversibility", *Mater. Today Energy*, **22** (2021) 100885.
17. Z. Li, P. Li, Q. Wan, F. Zhai, Z. Liu, K. Zhao, L. Wang, S. Lu, L. Zou, X. Qu, A. Volinsky, "Dehydrogenation improvement of $LiAlH_4$ catalyzed by Fe_2O_3 and Co_2O_3 nanoparticles", *J. Phys. Chem. C*, **117** [36] (2013) 18343–18352.
18. S. Wei, J. Liu, Y. Xia, H. Zhang, R. Cheng, L. Sun, F. Xu, P. Huang, F. Rosei, A. Pimerzin, H. J. Seifert, H. Pan, "Remarkable catalysis of spinel ferrite XFe_2O_4 (X = Ni, Co, Mn, Cu, Zn) nanoparticles on the dehydrogenation properties of $LiAlH_4$: An experimental and theoretical study", *J. Mater. Sci. Technol.*, **111** (2022) 189–203.
19. Y. Xia, S. Wei, Q. Huang, J. Li, X. Cen, H. Zhang, H. Chu, L. Sun, F. Xu, P. Huang, "Facile synthesis of $NiCo_2O_4$-anchored reduced graphene oxide nanocomposites as efficient additives for improving the dehydrogenation behavior of lithium alanate", *Inorg. Chem. Front.*, **7** (2020) 1257–1272.
20. M. Ismail, A.M. Sinin, C.K. Sheng, W.B.W. Nik, "Desorption behaviours of lithium alanate with metal oxide nanopowder additives", *Int. J. Electrochem. Sci.*, **9** (2014) 4959–4973.
21. M. Ismail, Y. Zhao, X.B. Yu, I.P. Nevirkovets, S.X. Dou, "Significantly improved dehydrogenation of $LiAlH_4$ catalysed with TiO_2 nanopowder", *Int. J. Hydrogen Energ.*, **36** [14] (2011) 8327–8334.
22. X. Shen, X. Zhang, Q. Xiao, H. Liu, "Catalytical enhancement on hydrogen production from $LiAlH_4$ by Fe-Fe_2O_3 addition", *Int. J. Hydrogen Energ.*, **47** (2022) 16964–16977.
23. M. Ismail, N.A. Sazelee, N.A. Ali, S. Suwarno, "Catalytic effect of $SrTiO_3$ on the dehydrogenation properties of $LiAlH_4$", *J. Alloys Compd.*, **85** (2021) 157475.
24. S. Wei, J. Liu, Y. Xia, H. Zhang, R. Cheng, L. Sun, F. Xu, Y. Bu, Z. Liu, P. Huang, K. Zhang, F. Rosei, A.A. Pimerzin, H.J. Seifert, "Enhanced hydrogen storage properties of $LiAlH_4$ by excellent catalytic activity

of $XTiO_3$@h-BN (X = Co, Ni)", *Adv. Funct. Mater.*, **32** (2022) 2110180.
25. Z. Ding, H. Li, L. Sha, "New insights into the solid-state hydrogen storage of nanostructured $LiBH_4$-MgH_2 system", *Chem. Eng. J.*, **385** (2020) 123856.
26. M. Dragojlović, I. Milanović, A. Gradišek, S. Kurko, M. Mitrić, A. Umićević, J. Radaković, K. Batalović, "Mechanochemical modification of $LiAlH_4$ with Fe_2O_3 - A combined DFT and experimental study", *Int. J. Hydrogen Energy* **46** (2021) 13070–13081.
27. J.R. Ares, K.-F. Aguey-Zinsou, M. Porcu, J.M. Sykes, M. Dornheim, T. Klassen, R. Bormann, "Thermal and mechanically activated decomposition of $LiAlH_4$", *Mater. Res. Bull.*, **43** (2008) 1263–1275.
28. A. Andreasen, T. Vegge, A.S. Pedersen, "Dehydrogenation kinetics of as-received and ball milled $LiAlH_4$", *J. Solid State Chem.*, **178** [12] (2015) 3672–3678.
29. D. Blanchard, H.W. Brinks, B.C. Hauback, P. Norby, "Desorption of $LiAlH_4$ with Ti-and V-based additives", *Mater. Sci. Eng. B*, **108** [1-2] (2004) 54–59.
30. C.M. Andrei, J.C. Walmsley, H.W. Brinks, R. Holmestad, B.C. Blanchard, D. Hauback, G.A. Botton "Analytical electron microscopy studies of lithium aluminum hydrides with Ti- and V-based additives", *J. Phys. Chem. B*, **109** [10] (2005) 4350–4356.
31. A.S. Vorokh, "Scherrer formula: Estimation of error in determining small nanoparticle size", *Nanosyst. Phys. Chem. Mater.*, **9** [3] (2018) 364–369.
32. LJ. Matović , S. Kurko, Ž. Rašković-Lovre, R. Vujasin, I. Milanović, S. Milošević, J. Grbović Novaković, "Assessment of changes in desorption mechanism of MgH_2 after ion bombardment induced destabilization", *Int. J. Hydrogen Energy*, **37** [8] (2012) 6727–6732.
33. J. Šestak, G. Berggren, "The study of the kinetics of mechanism of solid-state reactions at increasing temperatures", *Thermochim. Acta*, **3** [1] (1971) 1–12.
34. R.A. Varin, L. Zbroniec, "Decomposition behavior of unmilled and ball milled lithium alanate ($LiAlH_4$) including long-term storage and moisture effects", *J. Alloys Compd.*, **504** (2010) 89–101.